

Synthesis, Structural Characterization and Photocatalytic Activity of Iron-Doped Titanium Dioxide Nanopowders

Jordana H. Castillo¹, Francisco J. Rodriguez², Aurelio López-Malo¹, Enrique Sanchez-Mora³, Marco A. Quiroz¹ and Erick R. Bandala^{1,*}

¹Universidad de Las Américas Puebla, Sta. Catarina Martir, Cholula 72810 Puebla, Mexico

²CIDETEQ. Parque Tecnológico Querétaro, Sanfandila, Pedro Escobedo 76703 Querétaro, México

³Instituto de Física, Benemérita Universidad Autónoma de Puebla, Apdo. Postal J-48, Puebla, Pue México, 72570, México

Abstract: Iron-doped TiO₂ nanopowders with different doping amounts have been prepared by co-precipitation method followed by heat treatment. The obtained materials were structurally, morphologically and analytically characterized by X-ray diffraction (XRD), FT-Raman spectroscopy, diffuse reflectance spectroscopy (DRS) and energy dispersive X-ray spectroscopy (EDX) coupled to scanning electron microscopy (SEM). XRD analysis revealed the major presence of the anatase crystalline phase for iron-doped and undoped TiO₂. SEM confirmed particles sizes among the nanometer scale along with XRD data. The presence of iron ions was validated by EDX-SEM. Diffuse reflectance techniques were carried out to validate the shift of the band edge absorption spectrum of doped TiO₂ nanoparticles towards the visible region and to confirm the presence of iron atoms in the TiO₂ crystal lattice by the resulting variation of the band gap value of the doped materials. Photocatalytic activity of the nanoparticles under UV and visible radiation was evaluated by means of hydroxyl radicals production through indirect estimation using N,N-dimethyl-p-nitrosoaniline (PNDA) photo-discoloration experiments in aqueous dispersion. Samples containing 1.2 and 5.6 weight % Fe exhibited the highest activities in this study for both conditions.

Keywords: Doped titanium dioxide, anatase, photocatalytic degradation, iron doping.

1. INTRODUCTION

Since the first report on TiO₂ photocatalytic properties, research on heterogeneous photocatalytic processes for environmental restoration has been extensively reported [1-3]. Therefore, photocatalysis has become a major interest for research and technology development to accomplish higher mineralization rates of organic pollutants in underground, surface and wastewater. Furthermore, TiO₂ photocatalytic process allows the use of solar radiation for the disinfection and mineralization of a wide range of microorganisms and pollutants [4-7]. However, because its wide band gap energy (3.2 eV), TiO₂ is activated only by ultraviolet (UV) radiation with the consequent disadvantage for solar applications since UV radiation in the solar spectrum has been estimated in the range between 5-7%. During the last decades, several attempts in order to overcome this limitation and seek improvements for the process performance (reduction of irradiation time, increase of mineralization rates) have been reported. Among them, research on the modification of TiO₂, and doping of the semiconductor has been a subject of mayor interest. The goal of these efforts has been to reduce the

charge carriers (i.e. e^-/h^+) recombination rate and improve the photosensitivity of TiO₂-based semiconductors through red-shifting the optical absorption edge towards the visible spectral region by reducing its band-edge gap energy requirements for photocatalytic activation. These new materials could be activated by the energy of photons above 400 nm, which represents about 45% of the total solar radiation. The reduction of the energy photo-threshold is generally achieved by several catalyst modification techniques including dye sensitization, coupling TiO₂ with other semiconductors possessing favorable band gaps and potentials, surface deposition of metal clusters, and doping the crystal lattice with metallic (Fe, Co, Ag) and non-metallic foreign atoms (N, C, F, S). In recent years several papers have reported the extent of the photocatalytic activity of TiO₂ into the visible region when using iron as dopant [2, 3, 8, 9]. Regarding material size, interest in nanoscience and nanotechnology has increased during the last decades and research activities have focused on the synthesis and activity of new photocatalytic nanoparticles showing interesting properties and applications. New physical and chemical properties emerge when the size of the material becomes smaller and down to the nano-size scales. This is due to the well-studied quantum confinement ruling the transport of electron-hole pairs in semiconductor materials, and because size and geometry affect transport properties of photons [10].

*Address correspondence to this author at the Universidad de Las Américas Puebla, Sta. Catarina Martir, Cholula 72820 Puebla, Mexico; Tel: +522222292652; E-mail: erick.bandala@uldap.mx

Also, it is well known that smaller particles have larger specific surface area and surface/volume ratio becoming very attractive for AOPs since it facilitates the reaction between substrates and media.

In this work, highly efficient iron-doped TiO₂ nanoparticles were synthesized by the co-precipitation method followed by heat treatment. Co-precipitation method has been reported as a simple way to generate both perfect crystalline quality and large surface areas [11], however to our best knowledge it has not being reported for the synthesis of iron-doped TiO₂ nanoparticles. The aim of this work is to present the results on the detailed characterization and test photocatalytic capabilities of iron-doped TiO₂ nanoparticles synthesized by co-precipitation.

2. EXPERIMENTAL SECTION

2.1. Synthesis of Iron-Doped TiO₂ Nanoparticles

All chemicals used were of analytical reagent grade and used without further purification. All solutions were prepared with de-ionized distilled water. Pure TiO₂ and four different Fe-doped TiO₂ powders were prepared as follows: 3 g of titanium were dissolved in 80 mL of HCl (30% v/v) and kept overnight at room temperature. Then, the solution was heated at boiling temperature during 3 h and filtered. Concentrated HNO₃ was slowly added in the mixture under constant stirring. In agreement with Wang *et al.* [12], the dopant amount of iron-TiO₂ nanoparticles with the optimum performance in photocatalytic processes corresponds to iron doping at 0.10 -0.50 at.%. Accordingly, the amount of iron within the TiO₂ lattice was targeted to be 0.50 at.% by dissolving the proper amount of FeSO₄•7H₂O (1.20 iron%weight) to the above solution under constant vigorous stirring. Stirring was continued until a light brown solution formed. Finally NH₄OH was added dropwise into solution under constant stirring until obtaining a hydrogel. The resulting precipitates were washed with water, subsequently collected and lyophilized (Labconco, FreeZone 2.5 lyophilizer). Additionally to the material containing 0.50 at.% two other materials were synthesized including no iron dopant and 2.50 at.%, respectively for comparative purposes. The synthesized powders were then transferred to a muffle (Fisher Scientific, 10-650-14A), sinterized at 550 °C for 3h, and then air cooled to room temperature. In order to get insights into the structure of the particles, the obtained white (undoped) and yellow (Fe-doped) TiO₂ nanoparticles were then subjected to further characterization by several techniques.

2.2. Structural Characterization

Phase analysis and crystallite size of the particles were elucidated by X-ray diffraction (XRD). Measurements were performed at room temperature on a diffractometer (Bruker axs D8 Advance, Madison, WI, U.S) using nickel filtered CuK α radiation ($\lambda=1.54178\text{\AA}$) operating at 30kV and 40mA. The patterns were recorded over the range of 20-70° (2 θ) with a step size of 0.02° and at the speed of 1° min⁻¹.

Scanning electron microscopy (SEM) images of the nanoparticles were collected on a scanning electron microscope (March JEOL5400IV, Japan) operating at an acceleration voltage of 20 kV. Samples for SEM was deposited on carbon tapes. SEM images were used to observe the surface morphology of particles.

The energy dispersive X-ray spectroscopy (EDX) was measured with Noran software coupled to the above SEM and used for qualitative and quantitative analysis powders.

The UV-visible diffuse reflectance spectra (DRS) were acquired by using a UV-Vis-NIR spectrophotometer to validate the red shift of the edge in the nanoparticles. Data from the UV-visible DRS were used to estimate the band gap value for the synthesized materials using a plot of the modified Kubelka-Munk function (1):

$$f(R) = \frac{(1-R)^2}{2R} = \frac{\alpha}{S} \quad (1)$$

(where R is the reflectance and α and S are the absorption and scattering coefficients of the materials) versus the energy of the exciting light [13].

FT-Raman spectra were recorded in the range 100-1200cm⁻¹ on a spectrophotometer (UV-VIS LabRAMAN HR) equipped with a liquid-nitrogen-cooled charge-coupled device (CCD) detector, using for excitation a He-Ne (632.8 nm) laser.

2.3. Photocatalytic activity

The photocatalytic activity of the nanomaterials was tested for the photocatalytic discoloration of N,N-dimethyl-p-nitrosoaniline (PNDA), at atmospheric pressure and room temperature. PNDA photocatalytic discoloration assays were done by pouring the reagent in an open 250 mL Pyrex beaker on which the light beam was focused. The batch reactors were equipped with a magnetic stirring bar to ensure uniform mixing of

the solution in the vessel. An aqueous dispersion was prepared by adding the required amount of iron-doped or undoped particles to a 200mL solution containing the PNDA at appropriate concentration ($5 \times 10^{-5} \text{M}$) and 1gL^{-1} of catalyst under controlled pH (i.e. pH= 7.0) using a phosphate buffer solution. The aqueous suspensions were sonicated in the dark for 5 minutes before illumination to assure uniformity in the photocatalytic particles and attain adsorption equilibrium. The suspensions thus obtained were then irradiated. Samples were irradiated for 30 minutes using both, a low-pressure Hg lamp ($\lambda = 365 \text{ nm}$) with a radiation intensity of $0.378 \text{ mJcm}^{-2}\text{s}^{-1}$, and a visible light ($\lambda \geq 400 \text{ nm}$) irradiation lamp with the same radiation intensity to evaluate the effect of the radiation type on the process. Irradiation intensity was measured with a Solar Light Co., Inc radiometer PMA2100. During the irradiation, the suspensions were stirred at a constant speed. At any given irradiation time interval, aliquots of 4 mL of the solution were drawn to monitor the reaction progress. To perform the spectroscopic measurements the liquid samples were filtered through Millex[®]V 0.1 μm Low Protein Binding Durapore (PVDF) filters to separate TiO_2 particles. Photo discoloration of PNDA was followed by quantitative measurement of the compound concentrations using a HACH 02086 UV-Vis spectrophotometer and spectra were recorded. The UV-Vis spectrophotometer was set at the PNDA maximum absorption peak at the pH value tested (λ_{max} 440 nm at pH=7.0).

3. RESULTS AND DISCUSSIONS

3.1. Characterization of Iron-Doped and Undoped TiO_2 Nanoparticles

3.1.1. XRD

X-ray diffraction patterns, shown in Figure 1, suggested the major presence of anatase as the main phase on the powders. Diffractograms showed no significant difference on patterns among doped and undoped- TiO_2 powders. Incorporation of the iron into the structures of titanium and replaced titanium ion is assumed occurring since no iron oxide (Fe_xTiO_y) peak is observed in the XRD spectra ($2\theta \approx 35.0^\circ$ from JCPSD Card#19-629) as proposed previously [13, 14].

As shown in Figure 1, all samples were similar containing XRD peaks at 25.3° , 37.8° and 48.0° elucidating the (101), (004), and (200) TiO_2 anatase crystal structure. This indicated that the obtained nanoparticles exist in the anatase structure with dominated phase at 25.3° . Presence of iron ions seems to result in peak (101) broadening in comparison with undoped TiO_2 particles. No characteristic peaks of rutile-type phase (27.5°) are evident in any sample.

The crystallite sizes of the particles were estimated by applying the Debye-Scherrer diffraction equation:

$$D = \frac{K\lambda}{\beta \cos \theta} \quad (2)$$

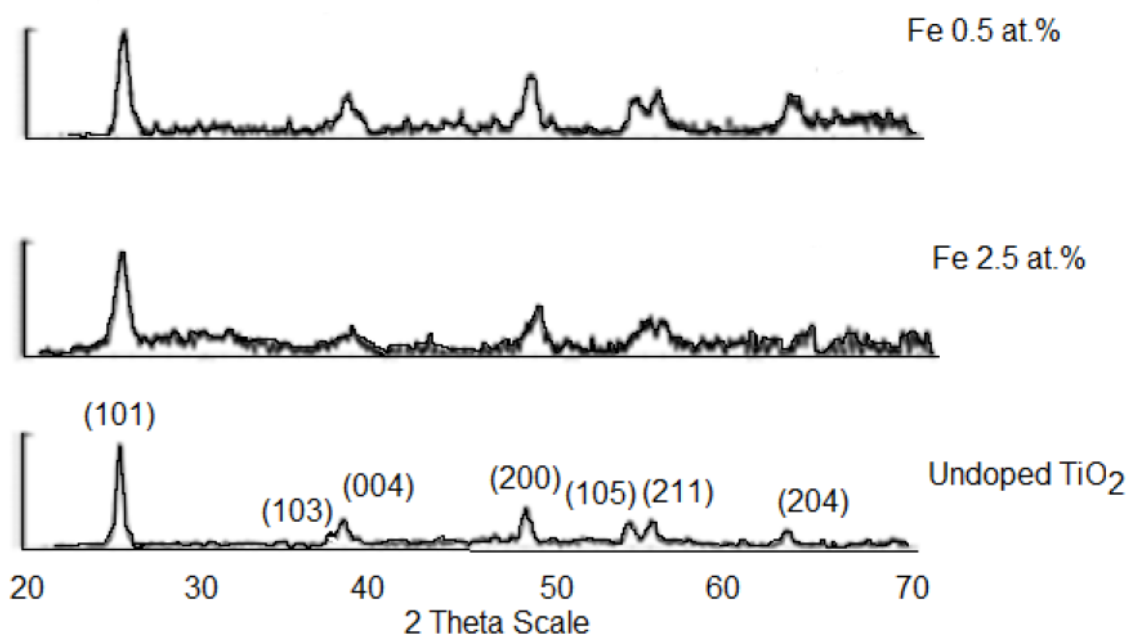


Figure 1: X-ray diffraction patterns of Fe-doped (0.5 and 2.5 at.%) and undoped TiO_2 .

Table 1: Crystallite Sizes and Elemental Composition of the Undoped and Iron-Doped TiO₂ Nano Powders Obtained

Sample	Particle Size*(nm)	Fe Content, at.%	Ti Content, at.%	O ₂ Content, at.%	E _g (eV)
0.5 at.%	1.39	0.50±0.11	23.39±5.81	60.68±12.5	2.68
2.5 at.%	1.37	2.48±0.15	24.69±3.80	72.84±3.93	1.87
Undoped	2.38	0.00	30.48±6.37	69.53±6.37	3.2

*From the Debye-Scherrer equation.

where D is the average crystallite size of the particles (nm), K is the coefficient taken to be as 0.94, λ is the X-ray wavelength of the Cu K α X-ray radiation ($\lambda=1.5406$ Å), β is the full width at half-maximum intensity of the diffraction peak observed at 2θ (radian), and θ is the Bragg's angle, using the most prominent peak of the major phase diffracting angle.

The average crystallite sizes of the iron-doped TiO₂ particles are smaller than undoped TiO₂ particles, these results are in agreement with previous reports [13, 14] where doping iron ions were found to contribute to lowering the sizes of the nanoparticles. Table 1 shows the specific data of the crystallite sizes, elemental analysis and band gap energy values for the synthesized undoped and iron-doped TiO₂ nanopowders.

3.1.2. EDX-SEM

SEM images and EDX were used jointly to elucidate the morphologies and elemental composition for the undoped and iron-doped TiO₂ nanoparticles. SEM images and measurements (Figure 2) revealed porous and relatively compact agglomerated microstructures with an average size of crystallites in the nanoscale range. As shown in Figure 2, nanoparticles generate agglomeration when removed from suspension for SEM analysis generating bigger particle conglomerates over 5 μ m size.

Energy dispersive spectroscopy (EDX) analysis was carried out to elucidate the elemental composition of the particles, and to validate the presence of iron ions in the particle. Figure 3 displays the EDX pattern confirming the presence of iron. Presence of iron ions

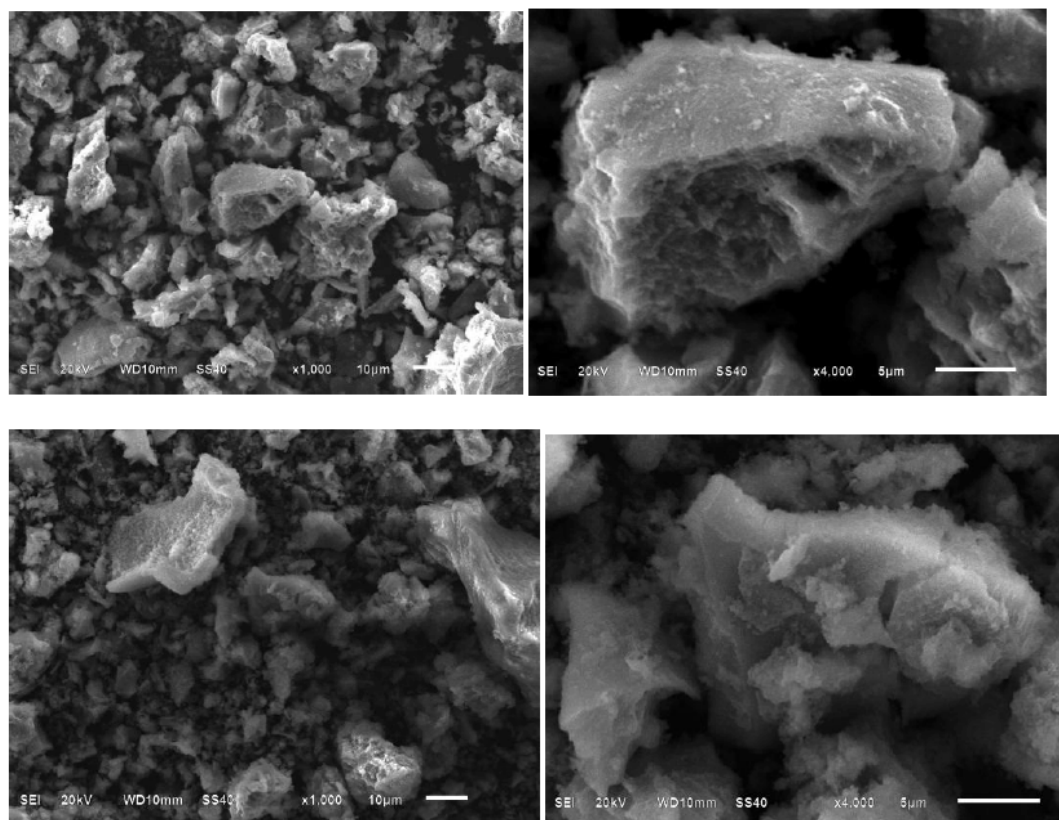


Figure 2: SEM image of 0.5 and 2.5 at. % w iron-doped TiO₂ particles.

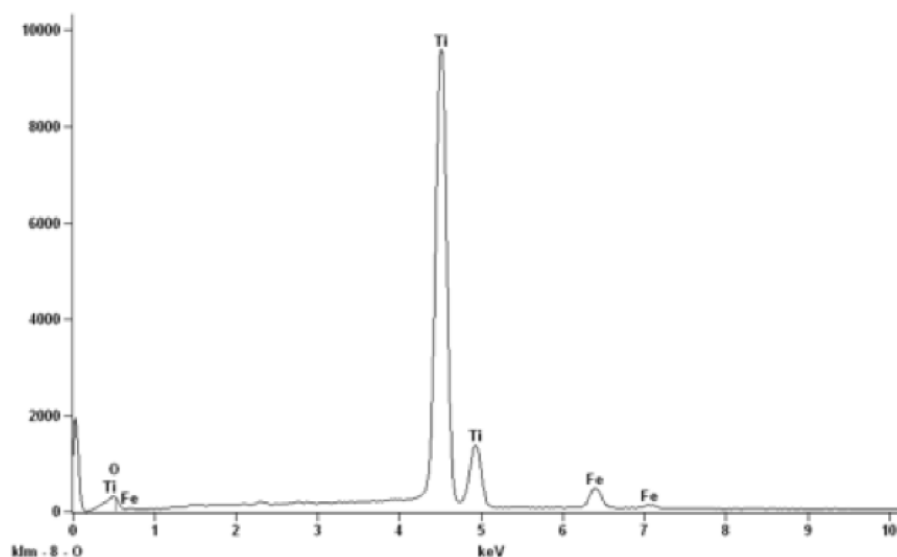


Figure 3: EDX-SEM pattern for 0.5 at.% w iron-doped TiO₂ nanoparticles confirming the presence of iron ions.

into the layer was also assumed from the change on the color of doped powders from light to dark yellow, as reported by Naeem and Ouyang [14].

3.1.3. UV-Visible Diffuse Reflectance Analysis

Doping TiO₂ nanoparticles with iron ions showed significant influence on optical properties of TiO₂, resulting on the shift of the absorption spectrum towards the visible region, as depicted in Figure 4. Doped TiO₂ revealed a single broad intense absorption as compared to undoped TiO₂, the light absorption properties of all doped samples changed and their edges expanded, consistent with previous reports [3,

15, 16]. It can be seen that the absorption edge of pure undoped TiO₂ is in the wavelength range 350-400 nm, which is in accordance with the reported by Ganesh *et al.* [16].

Fe₂O₃ absorption profile is also shown in Figure 4. The Fe₂O₃ DRS spectrum revealed three absorption bands in the ranges around 550-600, 650-700 and 800-1100 nm [15]. Iron doped TiO₂ composites exhibited increased degrees of absorbance and expanded edges that can be explained in terms of the gradual incorporation of iron ions into the lattice. Particles doped with 2.5 at.% of iron exhibited the highest

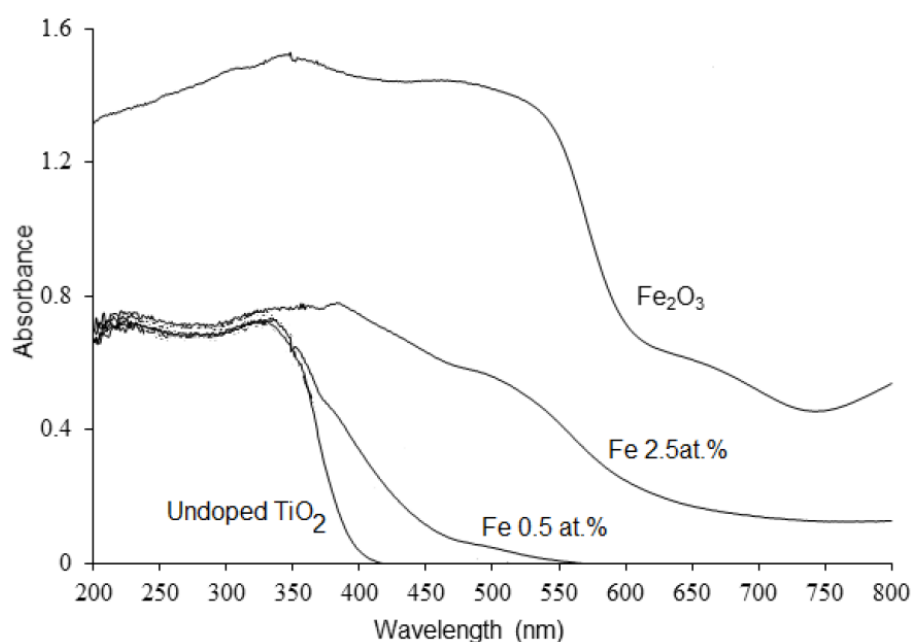


Figure 4: Diffuse reflective spectra showing the large red-shift of the optical absorption edge towards the visible spectral region.

Table 2: Radicals Production Rate (k) for UV and Visible Radiation in Aqueous Solutions of PNDA Using Undoped and Iron-Doped TiO₂ Nanoparticles, as a Function of the Accumulated Energy in the System

Sample	$k/10^3$ (min ⁻¹), UV Radiation	$k/10^3$ (min ⁻¹), Vis Radiation
0.5 at.% Fe	2.00, R ² = 0.98	1.20, R ² = 0.95
2.5 at.% Fe	2.20, R ² = 0.99	1.30, R ² = 0.97
Undoped TiO ₂	0.18, R ² = 0.99	-

absorbance consistent with the reported by Ganesh *et al.* [16]. UV-Vis DRS results are in agreement with previous reports on ligand field transitions overlapping the field transfer band tail. Absorbance profiles increased with higher amounts of doping. Nevertheless this behavior is not constant as previously reported [16]. This trend can be explained in terms of the catalyst modification having substitutional iron ion into the TiO₂ lattice or as surface deposition of Fe₂O₃ clusters. As shown in Figure 4, the increasing of iron-doping concentration generated increases in the absorbance. The red shift of the absorption edge in iron doped titania has been attributed to the charge-transfer transition between the iron ion d electrons and the TiO₂ conduction or valence band. It has been reported that metal doping could form a dopant energy level within the band gap of TiO₂. The electronic transition from the valence band to dopant level or from the dopant level to the conduction band can effectively red shift the band edge absorption threshold [24].

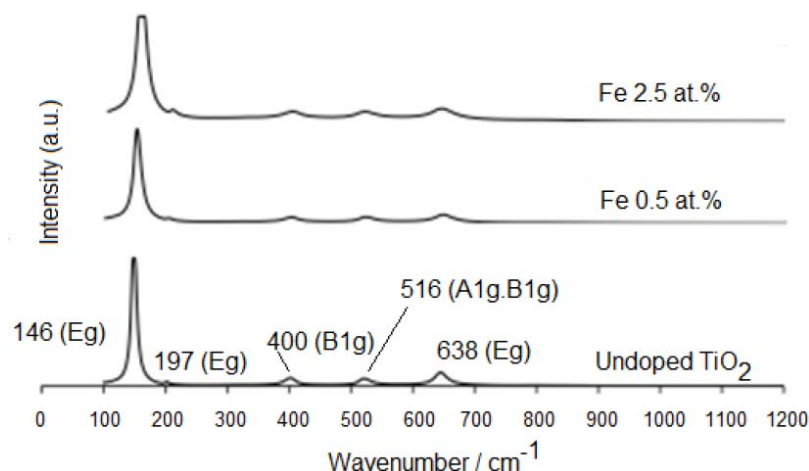
Decreases in the band gap energy (E_g) for the iron-TiO₂ materials synthesized shown in Table 2 supports also the proposed modifications to the titania lattice. It has been stated [17] that changes in the band gap values are consequence of a semiconductor: metal heterojunction. Considering this, low doping load (i.e. 0.5 at % Fe) in the TiO₂ may result mainly by the

inclusion of iron into the titania's crystallite lattice and the consequent spectra more similar to the one exhibited by undoped TiO₂. When high doping load (i.e. 2.5 at.% Fe) was tested, the observed radiation absorption spectra behave more likely iron oxide because the higher amount of surface deposition of Fe₂O₃ clusters.

3.1.4. RAMAN Analysis

FT-Raman profiles of undoped and iron doped TiO₂ nanoparticles are depicted in Figure 5. The five Raman active normal modes of vibration noted for the tetragonal anatase crystallite form of TiO₂ are centered at 146, 202, 400, 521, 528, 645 and 797 cm⁻¹. Profiles did not revealed presence of any rutile phase. These measurements are consistent with those reported by Balachandran and Eror [18] reporting absorption at 146, 198, 320, 398, 448, 516 and 640 cm⁻¹ for anatase TiO₂ Raman bands.

The frequencies for anatase TiO₂ in the iron-doped particles are centered at 145-153, 201-204, 398-402, 528 and 642-645 cm⁻¹, being the band around 146 cm⁻¹, attributed to the main E_g anatase vibration mode, the strongest. Iron ions into the lattice did not exhibited any other additional peaks consistent with previous reported [16] for iron doped TiO₂ powders. No peaks attributed to iron oxide were observed which is

**Figure 5: FT-Raman spectra of undoped and iron-doped TiO₂.**

consistent with results of the XRD patterns and supports the thesis of the inclusion of iron within the TiO_2 lattice [19].

3.2. Photocatalytic Activity

The photocatalytic activity of the undoped and iron-doped TiO_2 nanopowders was evaluated in terms of the photocatalytic discoloration of PNDA, used as test molecule, under UV and visible light irradiation. PNDA bleaching was used as indirect index of the production of free $\cdot\text{OH}$ radicals on undoped and iron-doped TiO_2 powders. PNDA was spectrophotometrically traced at 440 nm. From calibration by using the Beer's Law (Absorbance vs [PNDA] with $r^2 = 0.9975$) a molar absorptivity of $\epsilon_{440} = 33580 \text{ M}^{-1}\text{cm}^{-1}$ was obtained. Based on the results obtained from the PNDA-OH radicals trapping, the value of relative $\cdot\text{OH}$ radicals'

production rate (k) respect to the reaction time for the powders synthesized and tested, assuming a pseudo first-order reaction, as already proposed by Liu *et al.* [20] was estimated (see Table 2). Figures 6 and 7 shows the PNDA discoloration assays performed under UV and visible radiation, respectively.

Table 2 summarizes the values for the kinetic parameters estimated for the experimental values obtained from data in Figures 6 and 7. The experimental results showed that the presence of iron ions improved the photodiscoloration efficiency under both, UV and visible irradiation conditions (see Table 2).

For UV irradiation assays, the discoloration results obtained for both, iron doped and undoped TiO_2 nanopowders revealed only marginal

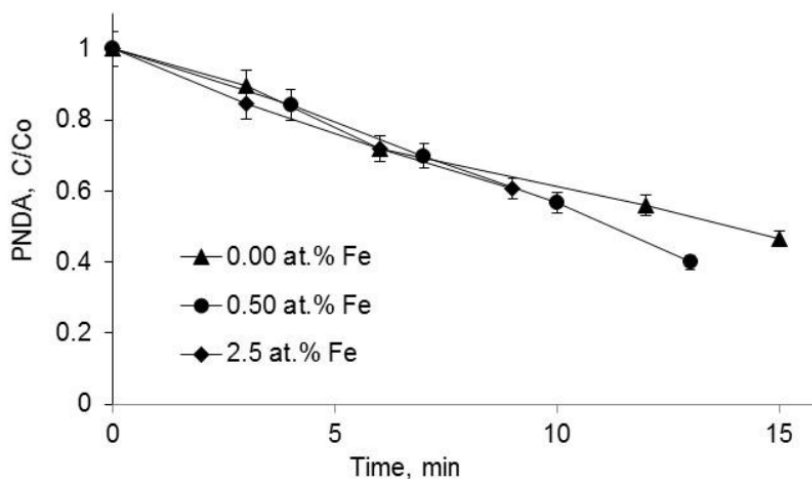


Figure 6: PNDA photocatalytic discoloration under UV radiation using undoped and iron-doped TiO_2 nanoparticles as a function of reaction time.

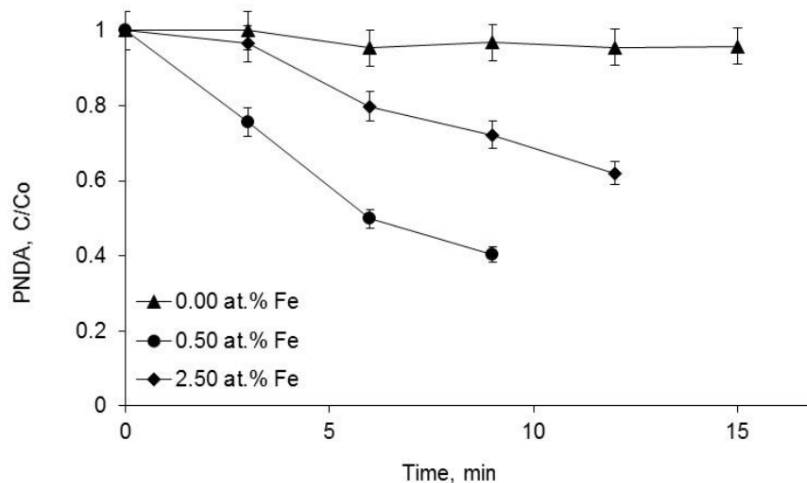


Figure 7: PNDA photocatalytic discoloration under visible radiation using undoped and iron-doped TiO_2 nanoparticles as a function of reaction time.

improvement. TiO₂ catalysts with iron doping showed a slightly higher photocatalytic activity for the discoloration of PNDA in the experiments performed with UV radiation. In agreement with previous reports [2, 23] metal ion doping influences the degradation efficiency of doped TiO₂ providing it may be presents at appropriate doping amounts. Iron doping is expected to generates electron or hole traps, when formed traps can cause the formation of some active species that benefit degradation of substrate, dopant introduction shows a positive effect. In these experiments iron doping decreases the photogenerated charge carriers (e⁻_{CB} and h⁺_{CV}) recombination rate, because of an electron scavenger effect taking place on the Fe³⁺ clusters, acting either as electron or hole traps, within both matrix as well as on the surface of doped TiO₂ through the replacement of Ti⁴⁺ by Fe³⁺, based on the favorable energy levels. Egerton *et al.* [21] have proposed that, at low iron levels, the photo-generated electrons are trapped at the surface iron centres. They proposed that higher iron levels will generate electron-hole recombination at iron centres becoming faster, reducing the number of available holes and, therefore, causing the degradation efficiency decrease, when the doping amount increases as shown in this work. At an appropriate doping concentration, iron ions may act as mediator for the transfer of interfacial charge, as result electron-hole pairs are temporarily separated more effectively than in undoped TiO₂ then responsible for the generation of ROS, leading to the photodegradation of substrates (PNDA in this case). Also, iron ions have an intense absorption in the UV-visible region and generate a red shift in the band gap transition of the iron-doped TiO₂ resulting in production of more photogenerated charge carriers to participate in photocatalytic reactions.

When visible radiation was used, the PNDA photocatalytic discoloration efficiency of iron doped TiO₂ was significantly higher than those observed for undoped TiO₂. The improvement of the photoactivity could be explained by the smaller crystallite sizes of the catalysts but mainly by the large red-shift in the light absorption edge of TiO₂ towards the visible region of the electromagnetic spectrum, resulting from the presence of the iron ions into the lattice that increase their photoabsorptive properties. These results lead to conclude that iron ions into the powders edge-shift to wavelengths over 400nm and decrease band gaps, as reported previously [2, 3, 22]. However, photocatalytic discoloration rate only increased slightly when the iron amount reaches the highest level (i.e. 2.50 at % Fe).

When dopant introduction cannot decrease the e⁻_{CB} and h⁺_{CV} recombination rate, then the introduction is ineffective for degradation. It is important to note that eventhough no significant degradation rate increases were observed when high dopant level were tested, it is still fairly higher than pure TiO₂ photoactivity.

4. CONCLUSIONS

Pure TiO₂ and two different iron-doped TiO₂ nanoparticles were prepared by the co-precipitation method, followed by a heat treatment. XRD, EDX-SEM, diffuse reflectance spectroscopy and FT-Raman analysis techniques were used in the characterization of the obtained nanoparticles. X-ray diffraction patterns confirmed that the iron-doped and undoped nanometer crystals possess exclusively the TiO₂ anatase-type structures. SEM images showed porous microagglomerates. EDX results validated the presence of iron ions into the samples and revealed their elemental composition. DRS results validated the large red-shift of the absorption spectra and the decrease in band gap energy for iron-containing TiO₂ nanoparticles which was related with the inclusion of iron in the TiO₂ crystallite lattice. Photocatalytic activity was evaluated and the experiments revealed the influence of metal ion doping on it. The iron-TiO₂ nanoparticles showed the highest photocatalytic efficiencies under UV and visible light irradiation assays. Iron ions were found influencing the photocatalytic discoloration efficiencies due to their scavenger effect, diminishing the recombination rates of the electron-hole pairs, and increasing the UV-visible light absorption.

ACKNOWLEDGEMENTS

This work was partially funded by the National Council of Science and Technology, CONACyT (México) grant CB-2011-01-168285. J.Castillo-Ledezma gratefully acknowledges the scholarship received from CONACyT (México) and Universidad de las Américas Puebla (México) for her Doctoral studies.

REFERENCES

- [1] Cernea M, Secu M, Secu CE, Baibarac M, Vasile BS. Structural and thermoluminescence properties of undoped and Fe-doped TiO₂ nanopowders processed by sol-gel method. *J Nanopart Res* 2011; 13: 77-85. <http://dx.doi.org/10.1007/s11051-010-0002-7>
- [2] Popa M, Diamandescu L, Vasiliu F, *et al.* Synthesis, structural characterization, and photocatalytic properties of iron-doped TiO₂ aerogels. *J Mat Sci* 2009; 44: 358-64. <http://dx.doi.org/10.1007/s10853-008-3147-3>

- [3] Zhang Y, Lv F, Wu T, *et al.* F and Fe co-doped TiO₂ with enhanced visible light photocatalytic activity. *J Sol-Gel Sci Technol* 2011; 59: 387-91.
<http://dx.doi.org/10.1007/s10971-011-2449-0>
- [4] Bandala ER, Gelover S, Leal MT, Arancibia C, Jiménez A, Estrada CA. Solar photocatalytic degradation of Aldrin. *Catal Today* 2002; 76: 189-99.
[http://dx.doi.org/10.1016/S0920-5861\(02\)00218-3](http://dx.doi.org/10.1016/S0920-5861(02)00218-3)
- [5] Byrne JA, Fernández-Ibañez P, Dunlop PS, Alrousan DM, Hamilton JW. Photocatalytic enhancement for the solar disinfection of water: a review. *Int J Photoen* 2011.
<http://dx.doi.org/10.1155/2011/798051>
- [6] Fernandez P, Blanco J, Sichel C, Malato S. Water disinfection by solar photocatalysis using compound parabolic collectors. *Catal Today* 2005; 101: 345-56.
<http://dx.doi.org/10.1016/j.cattod.2005.03.062>
- [7] Villafán HI, Cuevas SA, Arancibia CA. Modeling the solar photocatalytic degradation of dyes. *J Solar Ener Engin* 2007; 129: 87-93.
<http://dx.doi.org/10.1115/1.2391255>
- [8] Irie H, Watanabe Y, Hashimoto K. Nitrogen-concentration dependence on photocatalytic activity of TiO₂-xN_x powders. *J Phys Chem B* 2003; 130: 163-70.
- [9] Yu JC, Tang HY, Chan HC, *et al.* Bactericidal and photocatalytic activities of TiO₂ thin films prepared by sol-gel and reverse micelle methods. *J Photochem Photobiol A: Chem* 2002; 153: 211-9.
[http://dx.doi.org/10.1016/S1010-6030\(02\)00275-7](http://dx.doi.org/10.1016/S1010-6030(02)00275-7)
- [10] Abazovic ND, Mirengi L, Jankovic IA, *et al.* Synthesis and Characterization of Rutile TiO₂ Nanopowders Doped with Iron Ions. *Nano Res Lett* 2009; 4: 518-25.
<http://dx.doi.org/10.1007/s11671-009-9274-1>
- [11] Wang Z, Huang B, Dai Y, *et al.* Highly photocatalytic ZnO/In₂O₃ heterostructures synthesized by coprecipitation method. *J Phys Chem C* 2009; 113: 4612-7.
<http://dx.doi.org/10.1021/jp8107683>
- [12] Wang C, Bahnemann D, Dohrmann J. A novel preparation of iron-doped TiO₂ nanoparticles with enhanced photocatalytic activity. *Chem Commun* 2000; 16: 1539-40.
<http://dx.doi.org/10.1039/b002988m>
- [13] Cong Y, Zhang J, Chen F, Anpo M, He D. Preparation, photocatalytic activity and mechanism of nano TiO₂, co-doped with nitrogen and iron (III). *J Phys Chem C* 2007; 111: 10618-23.
<http://dx.doi.org/10.1021/jp0727493>
- [14] Naeem K, Ouyang F. Preparation of Fe³⁺-doped TiO₂ nanoparticles and its photocatalytic activity under UV light. *Sci Direct Phys B* 2009.
<http://dx.doi.org/10.1016/j.physb.2009.08.060>
- [15] Sanchez-Mora E, Gomez E, Rojas E, Silva R. Morphological, optical and photocatalytic properties of TiO₂-Fe₂O₃ multilayers. *Solar Ener Mat Solar Cells* 2007; 91: 1412-5.
<http://dx.doi.org/10.1016/j.solmat.2007.05.010>
- [16] Ganesh I, Kumar PP, Gupta AK, *et al.* Preparation and characterization of Fe-doped TiO₂ powders for solar light response and photocatalytic applications. *Process Appl Ceram* 2012; 6: 21-36.
<http://dx.doi.org/10.2298/PAC1201021G>
- [17] Cerro-Lopez M, Meas-Vong Y, Mendez-Rojas MA, Martinez-Huitile CA, Quiroz MA. Formation and growth of PbO₂ inside TiO₂ nanotubes for environmental applications. *Appl Catal B: Environ* 2014; 144: 174-81.
<http://dx.doi.org/10.1016/j.apcatb.2013.07.018>
- [18] Balachandran U, Eror NG. Raman spectra of titanium dioxide. *J Solid State Chem* 1982; 42: 276-82.
[http://dx.doi.org/10.1016/0022-4596\(82\)90006-8](http://dx.doi.org/10.1016/0022-4596(82)90006-8)
- [19] Liu F, He H, Zhang C. Novel iron titanate catalyst for the selective catalytic of NO with NH₃ in the medium temperature range. *Chem Comm* 2008; 17: 2043-5.
<http://dx.doi.org/10.1039/b800143j>
- [20] Liu Y, Liu H, Ma J, Wang X. Comparison of degradation mechanism of electrochemical oxidation of di- and trinitrophenols on bi-doped lead dioxide electrode: Effect of the molecular structure. *Appl Catal B: Environ* 2009; 91: 284-99.
<http://dx.doi.org/10.1016/j.apcatb.2009.05.039>
- [21] Egerton TA, Kosa SAM, Christensen PA. Photoelectrocatalytic disinfection of E. coli suspensions by iron doped TiO₂. *Phys Chem Chem Phys* 2006; 8: 398-406.
<http://dx.doi.org/10.1039/b507516e>
- [22] Ohno T, Tabigawa K, Fujimara K, Izumi S, Matsumara M. Photocatalytic oxidation of water by visible light using ruthenium-doped titanium dioxide powder. *J Photochem Photobiol A: Chem* 1999; 127: 107-11.
[http://dx.doi.org/10.1016/S1010-6030\(99\)00128-8](http://dx.doi.org/10.1016/S1010-6030(99)00128-8)
- [23] Bajamundi CJE, Dalida PML, Wantala K, Khemthong P, Grisdanurak N. Effect of Fe³⁺ on the performance TiO₂ mechanocoatedalumnia bead photocatalyst. *Korean J Chem Engin* 2011; 28: 1688-92.
<http://dx.doi.org/10.1007/s11814-011-0031-7>
- [24] Lü X, Mou X, Wu J, *et al.* Improved-performance dye-sensitized solar cells using Nb-doped TiO₂ electrodes: Efficient electron injection and transfer. *Adv Funct Mat* 2010; 20: 505-15.
<http://dx.doi.org/10.1002/adfm.200901292>